

The H α line as a probe of chromospheric magnetic fields

HARSH MATHUR ¹, JAYANT JOSHI ¹, THORE ESPEDAL MOE ^{1,2,3}, TIAGO M. D. PEREIRA ^{2,3} AND K. NAGARAJU ¹

¹*Indian Institute of Astrophysics, II Block, Koramangala, Bengaluru 560 034, India*

²*Institute of Theoretical Astrophysics, University of Oslo, P.O. Box 1029 Blindern, NO-0315 Oslo, Norway*

³*Rosseland Centre for Solar Physics, University of Oslo, P.O. Box 1029 Blindern, NO-0315 Oslo, Norway*

ABSTRACT

We explore the diagnostic potential of the H α line for probing the chromospheric magnetic field using a realistic 3D radiative magnetohydrodynamic (rMHD) model. The Stokes profiles of the H α line are synthesized through full 3D radiative transfer under the field-free approximation, alongside the Ca II 8542 Å and Fe I 6173 Å lines for comparison. The line-of-sight (LOS) magnetic fields are inferred using the weak field approximation (WFA) for the H α and Ca II 8542 Å lines, while the Fe I 6173 Å line is analyzed through Milne-Eddington inversion techniques. The comparison between the inferred LOS magnetic field maps and the magnetic fields in the rMHD model revealed that the H α line core primarily probes the chromospheric magnetic field at $\log \tau_{500} = -5.7$, which corresponds to higher layers than the Ca II 8542 Å line core, which is most sensitive to conditions at $\log \tau_{500} = -5.1$. On average, the Stokes V profiles of the H α line core form 500 km higher than those of the Ca II 8542 Å line core. The H α polarization signals persist after adding noise, and with noise at the level of $10^{-3} I_c$, most simulated magnetic structures remain visible. These findings suggest that spectropolarimetric observations of the H α line can provide complementary insights into the stratification of the magnetic field at higher altitudes, especially when recorded simultaneously with widely used chromospheric diagnostics such as the Ca II 8542 Å line.

Keywords: Solar magnetic fields, Solar chromosphere, Spectropolarimetry

1. INTRODUCTION

The H α spectral line serves as a key diagnostic tool for probing the solar chromosphere and its dynamic phenomena, including filaments, Ellerman bombs, surges, flares, and spicules. These events exhibit distinct spectral signatures that manifest in the H α intensity profiles, which are then used for the classification of solar features and for studying the fine structure and temporal evolution of the chromosphere.

Despite being a critical line to study the structure and evolution of the chromosphere, polarization studies to infer the magnetic field from this line remain limited. For instance, Abdussamatov (1971) utilized simultaneous measurements of the Fe I 6302.5 Å and H α lines to estimate vertical magnetic field gradients. Various studies have also documented simultaneous spec-

tropolarimetric observations of the H α line alongside Fe I lines, enabling comparative analyses of photospheric and chromospheric magnetic fields in sunspots (Balasubramaniam et al. 2004; Hanaoka 2005; Nagaraju et al. 2008). Radial variations of the line-of-sight magnetic field in both the chromosphere and photosphere of a sunspot were analyzed by Nagaraju et al. (2020). Furthermore, spectropolarimetric observations of the H α line have been employed to diagnose magnetic fields in prominences (López Ariste et al. 2005). Recently, Jaume Bestard et al. (2022) explored linear and circular polarization signals near the North and South Solar Limb, inferring the line-of-sight magnetic field through the weak field approximation (WFA).

The reason the H α line is not commonly used to infer chromospheric magnetic fields is due to its sensitivity to the complex 3D radiation field. While the Zeeman effect largely influences the Stokes V signal, both the intensity and polarization profiles of this line are highly sensitive to the complex 3D radiation field (Leenaarts et al. 2012), which makes accurate modeling—and con-

sequently, the interpretation of its observations—highly challenging. Additionally, in weakly magnetized atmospheres, the Stokes Q & U signals are affected by atomic polarization (Štěpán & Trujillo Bueno 2010, 2011), making the $H\alpha$ line difficult to model with current inversion codes, which typically rely on a 1.5D plane-parallel geometry. Furthermore, in weak-field conditions—where Zeeman splitting ($\Delta\lambda_B$) is significantly smaller than the Doppler width ($\Delta\lambda_D$)—the amplitude of circular polarization is proportional to the ratio of $\Delta\lambda_B$ to $\Delta\lambda_D$, while linear polarization scales with the square of this ratio (see Landi Degl’Innocenti & Landolfi 2004, p. 405)). This ratio is generally small for hydrogen, given its low atomic mass and correspondingly large Doppler width, in contrast to heavier atoms like calcium.

Socas-Navarro & Uitenbroek (2004) previously calculated 1D response functions of the $H\alpha$ line’s Stokes parameters, showing that it is notably sensitive to both photospheric and chromospheric magnetic fields. However, Leenaarts et al. (2012) demonstrated that a 1D radiative transfer approach is inadequate for accurately modeling the $H\alpha$ line. Only when the radiative transfer is treated in 3D, does the $H\alpha$ line appear to trace chromospheric magnetic structures like fibrils. Additionally, Carlsson & Stein (2002) showed that in the upper chromosphere, the $H\alpha$ line’s opacity is mainly sensitive to the ionization degree and radiation field, which are largely insensitive to the local temperature variations but are sensitive to mass density (Leenaarts et al. 2012). Recent work by Bjørgen et al. (2019) further confirmed the persistence of $H\alpha$ opacity in flaring active regions by synthesizing spectra using 3D radiative MHD simulations. Consequently, simultaneous spectropolarimetric observations of the $H\alpha$ line with well-established chromospheric diagnostics, such as those of the Ca II and He I atoms (Lagg et al. 2017), present a robust probe for investigating chromospheric magnetic fields.

Recent studies by Mathur et al. (2023, 2024) have utilized simultaneous spectropolarimetric observations of the $H\alpha$ and Ca II 8542 Å (and 8662 Å) lines to investigate the stratification of the chromospheric magnetic field by applying the weak-field approximation to the line core and wings, separately. In the study, Mathur et al. (2023) found that the line-of-sight (LOS) magnetic field morphology in the $H\alpha$ line core closely resembles that of the Ca II 8542 Å line, though it appeared more diffuse, and the inferred magnetic field strength was consistently weaker than that of the Ca II 8542 Å line. However, these observations were limited to a small pore. In the subsequent study, of a complex active region, Mathur et al. (2024) observed that the LOS magnetic fields inferred from the $H\alpha$ line core were uncor-

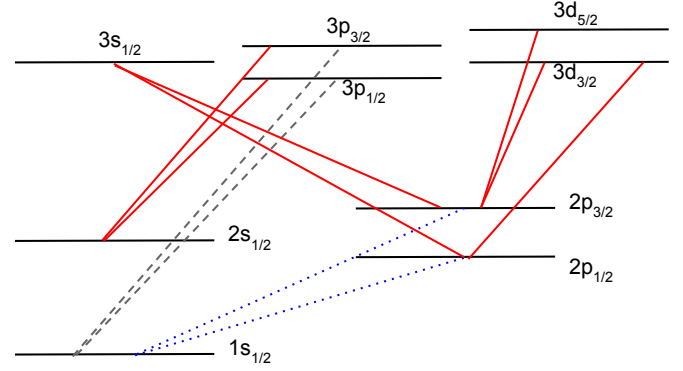


Figure 1. Grotrian diagram of Hydrogen atom showing the $H\alpha$ line is a combination of 7 transitions. The solid red-colored transitions correspond to the $H\alpha$ line, while the dotted blue-colored transitions correspond to Ly α and the dashed grey-colored transitions correspond to the Ly β line.

related, similarly diffuse, and consistently weaker than those from the Ca II 8662 Å and Fe I 8661.8991 Å lines. The weaker and more diffuse fields inferred from the line core, combined with the assumption that magnetic fields expand with height, led the authors to conclude that the $H\alpha$ line core is a reliable probe of the chromospheric magnetic field.

In this letter, we present a theoretical investigation into the diagnostic potential of the $H\alpha$ line for probing the chromospheric magnetic field. Using a publicly available 3D radiative magnetohydrodynamic (rMHD) simulation, we synthesize the Stokes profiles of the $H\alpha$ line through full 3D radiative transfer in field-free approximation. For comparison, we also synthesize the Stokes profiles of the Ca II 8542 Å and Fe I 6173 Å lines. To infer the LOS magnetic field, we apply the WFA to the $H\alpha$ and Ca II 8542 Å lines, and the Milne-Eddington inversion to the Fe I 6173 Å line. We then compare the morphology and field strengths of the inferred LOS magnetic field maps with the true fields in the 3D rMHD model.

2. MODELING THE POLARIZATION PROFILES OF THE $H\alpha$, Ca II 8542 Å AND Fe I 6173 Å LINES

To model the polarization profiles of the $H\alpha$ line in 3D, we have used a publically available enhanced network simulation (Carlsson et al. 2016) computed using the Bifrost Code (Gudiksen et al. 2011). This simulation used an equation of state that includes the effects of non-equilibrium ionization of Hydrogen. Using the simulation, we computed the hydrogen level populations using the *Multi3d* code (Leenaarts & Carlsson 2009), assuming a 6-level hydrogen atom (5 bound n -levels plus continuum), the same as those used in the Leenaarts et al.

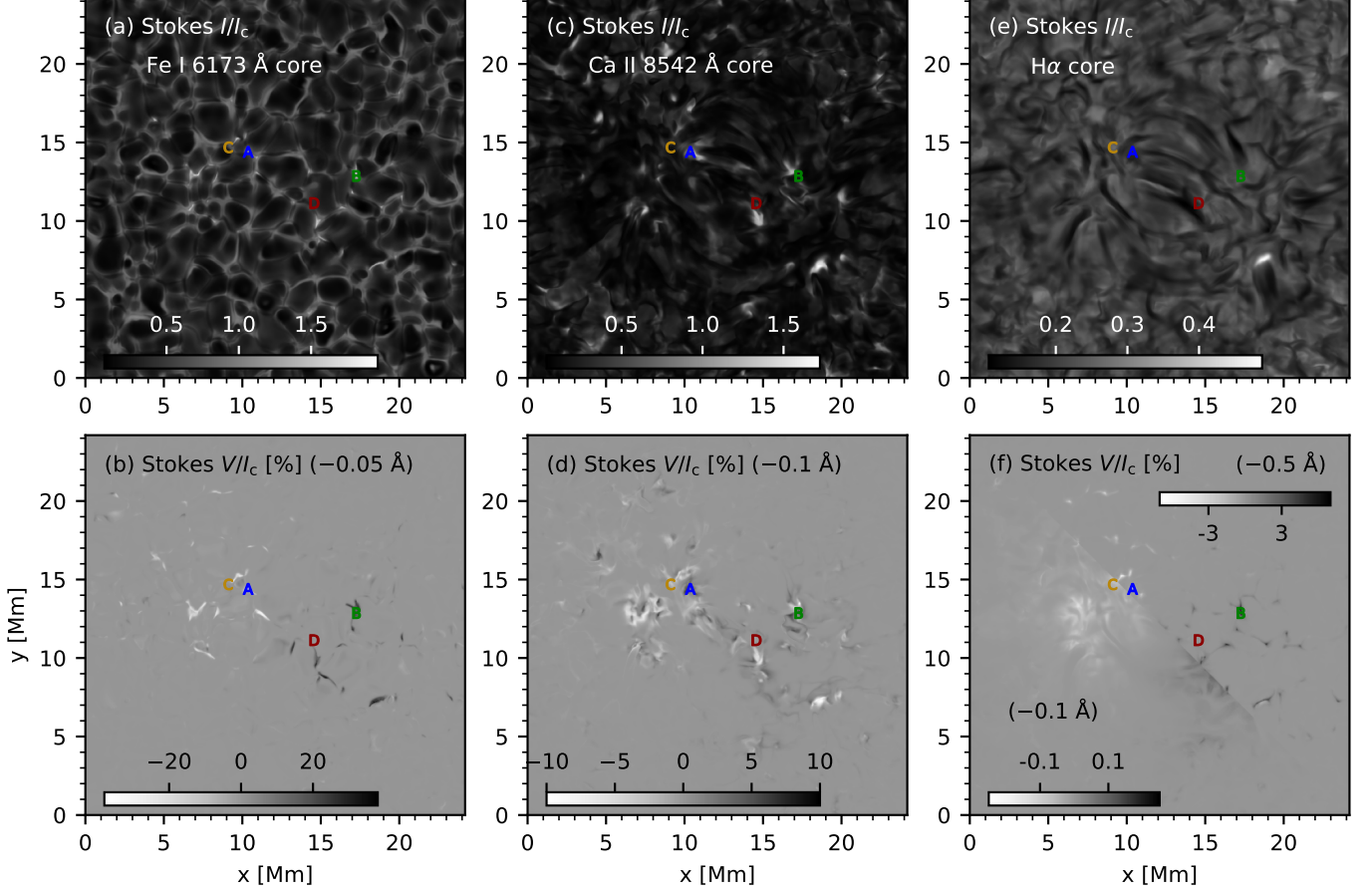


Figure 2. Synthetic Stokes I/I_c and Stokes V/I_c maps. The Stokes I/I_c maps in the top row (panels (a), (c), and (e)) are shown at the line core of the Fe I 6173 Å, Ca II 8542 Å, and H α lines. Panels (b) and (d) represent Stokes V/I_c at -0.5 Å and -0.1 Å for the Fe I 6173 Å and Ca II 8542 Å line, respectively. The top-right diagonal half of panel (f) displays the Stokes V/I_c image at -0.5 Å from the H α line core, while the bottom-left diagonal half presents the Stokes V/I_c image at -0.1 Å from the H α line core. Spectral profiles at a few selected pixels are shown in Fig. 3.

(2012) study. While the version of *Multi3d* we used can compute intensity profiles in 3D, it does not handle polarization. Additionally, to compute polarization, fine-structures (nlj) states of n levels must be included in the computation. The H α line is a combination of 7 transitions between the fine-structure states of $n = 3$ to $n = 2$ as shown in Fig. 1. To account for this, we redistributed the populations into a 9-level hydrogen atom, as illustrated in Fig. 1. The population of each n -level was redistributed across the fine-structure nlj -states in proportion to their statistical weights, ensuring that the density matrix elements of all nlj -states corresponding to the same n -level remain the same. These populations are then held constant for the subsequent calculation of polarization profiles, an approach known as the “field-free” approximation. We used the collisional rates given by Przybilla & Butler (2004) for this model hydrogen atom. This model atom is then used with the RH code (Uitenbroek 2001), on a column-by-column basis (also

known as 1.5D approximation) to do just the formal solution to calculate the emergent intensity and polarization profiles along the line-of-sight (LOS) at $\mu = 1$. We reiterate that the above step done using the RH code, did not modify the level populations.

To calculate the polarization profiles of the Fe I 6173 Å and Ca II 8542 Å lines, the RH code is again used under the 1.5D approximation. The Fe I 6173 Å is synthesized using Kurucz data (Kurucz 2011) under the local thermodynamic equilibrium (LTE) approximation. Recent studies have inferred the LOS magnetic field from the Fe I 6173 Å line using the LTE approximation (for eg. Pastor Yabar et al. 2020; Yadav et al. 2021; Joshi & Rouppe van der Voort 2022; Mathur et al. 2022). However, we note that Smitha et al. (2023), using a realistic 3D MHD simulation of a non-grey sunspot cube (Rempel 2012) generated with the MURaM code (Vögler et al. 2005), showed that LTE approximation may lead to underestimating the LOS magnetic field. The Ca II IR

lines were synthesized with the complete re-distribution (CRD) approximation using a 6-level Ca II atom. The polarization profiles of the Ca II 8542 Å line were also synthesized in “field-free” approximation, because we do not expect the magnetic field to influence the populations. While solving the radiative transfer for the Ca II 8542 Å and Fe I 6173 Å lines, the populations of the nlj -levels of the hydrogen atom were kept fixed to the populations calculated from the *Multi3d* code, as explained in the previous paragraph.

3. DESCRIPTION OF SYNTHETIC STOKES I AND V MAPS AND PROFILES OF THE $H\alpha$ LINE

Figure 2 shows the synthesized intensity and Stokes V/I_c maps in the Fe I 6173 Å, Ca II 8542 Å and $H\alpha$ lines. Where I_c represents the median intensity calculated separately for each spectral line across a region in the FOV with no magnetic activity, at a wavelength point -4 Å away from the line center for the Ca II 8542 Å and $H\alpha$ lines, and -2 Å away from the line center for the Fe I 6173 Å line. The Stokes I/I_c image for the Fe I 6173 Å line core displays a reverse granulation pattern, while the Stokes V/I_c image reveals the structure of the magnetic field network and magnetic field concentrated in intergranular lanes (see panels a and b), with a maximum amplitude of about 36%. For the Ca II 8542 Å line core, the Stokes I/I_c image captures the chromospheric fibrillar structure, whereas the Stokes V/I_c image depicts a diffuse magnetic field structure indicative of the chromosphere (see panels c and d), with a maximum amplitude of approximately 9.5%. In the $H\alpha$ line core, the Stokes I/I_c image resembles the top-left panel of Fig. 7 from Leenaarts et al. (2012). The Stokes V/I_c map of the $H\alpha$ line core at the wavelength position corresponding to the maximum amplitude of the Stokes V/I_c profiles (see Fig. 3), -0.5 Å, is shown in the top-right diagonal half of panel (f). This map exhibits a pattern similar to the network fields found in the simulation, with a maximum amplitude of 6.5%. The map at -0.1 Å bottom-left diagonal half of panel (f), shows a more diffuse structure than that in the Stokes V/I_c map (panel (d)) for the Ca II 8542 Å line. The V/I_c map at -0.1 Å in the $H\alpha$ line has maximum amplitude of 0.2%. To compare with active region observations reported in Mathur et al. (2024), the maximum amplitude observed in the Stokes V/I_c profiles of the $H\alpha$ line at the wavelength position corresponding to the maximum amplitude of Stokes V was observed to be 3%.

The spectral profiles of 4 selected pixels, marked by ‘A’, ‘B’, ‘C’ and ‘D’ in Fig. 2, are shown in Fig. 3. The Stokes I/I_c profiles for the Ca II 8542 Å and $H\alpha$ lines

are plotted in the first and third columns, respectively, while the Stokes V/I_c profiles for these lines are presented in the second and fourth columns. Additionally, the derivative of the Stokes I/I_c ($\frac{dI/I_c}{d\lambda}$, shown with dashed lines) is overplotted on the Stokes V/I_c profiles. The stratification of the LOS magnetic field of these 4 pixels is shown in panels (A), (B), (C), and (D) of Fig. 8 of the Appendix A, respectively. In this simulation, the LOS magnetic field follows the convention where positive values indicate an outward-directed field, consistent with the positive direction of the z -axis.

The spectral profiles shown in blue color, pixel ‘A’, represent a pixel where the LOS magnetic field consistently has a negative sign throughout all heights of the atmosphere. Notably, the Stokes V/I_c profile of the Ca II 8542 Å line exhibits multiple lobes and sign changes from the wings to the core, which might give an impression that magnetic field polarity is reversed from the photosphere to the chromosphere. However, this sign change aligns with the sign change in the derivative of Stokes I/I_c of the Ca II 8542 Å line, indicating no change in magnetic polarity with height. The Stokes I/I_c profiles of the $H\alpha$ line display nominal absorption, and the blue wing of the Stokes V/I_c profile for the $H\alpha$ line shows a negative sign, accurately indicating the pixel’s negative magnetic field polarity.

The spectral profiles shown in green color, pixel ‘B’, represent a pixel where the LOS magnetic field consistently has a positive sign. The Stokes I/I_c profiles of both the Ca II 8542 Å and $H\alpha$ lines show nominal absorption and blue wing of the Stokes V/I_c profiles show a positive sign, accurately indicating the pixel’s positive magnetic polarity.

The spectral profiles shown in brown color, pixel ‘C’, represent a pixel where the LOS magnetic field is positive in the lower photospheric layers ($\log \tau_{500} > -1.8$) and negative in the upper photospheric and chromospheric layers ($\log \tau_{500} < -1.8$). The corresponding Ca II 8542 Å Stokes V/I_c profile is complex showing multiple lobes. The blue lobe of the Stokes V/I_c profile for the Ca II 8542 Å line shows only a negative sign, which does not reflect the positive polarity of the lower photosphere. However, it is possible that a signature of the lower photospheric magnetic field might be hidden in this complex profile. Or it may also be possible that the wings of the Ca II 8542 Å line probe higher photospheric heights than those probed by the Fe I 6173 Å line. In contrast, the $H\alpha$ line has a typical two lobed Stokes V/I_c profile. Moreover, the sign of Stokes V/I_c profiles shifts from positive to negative around ~ -0.5 Å, clearly indicating that the $H\alpha$ line is capturing magnetic polarity reversal with height with wings sampling

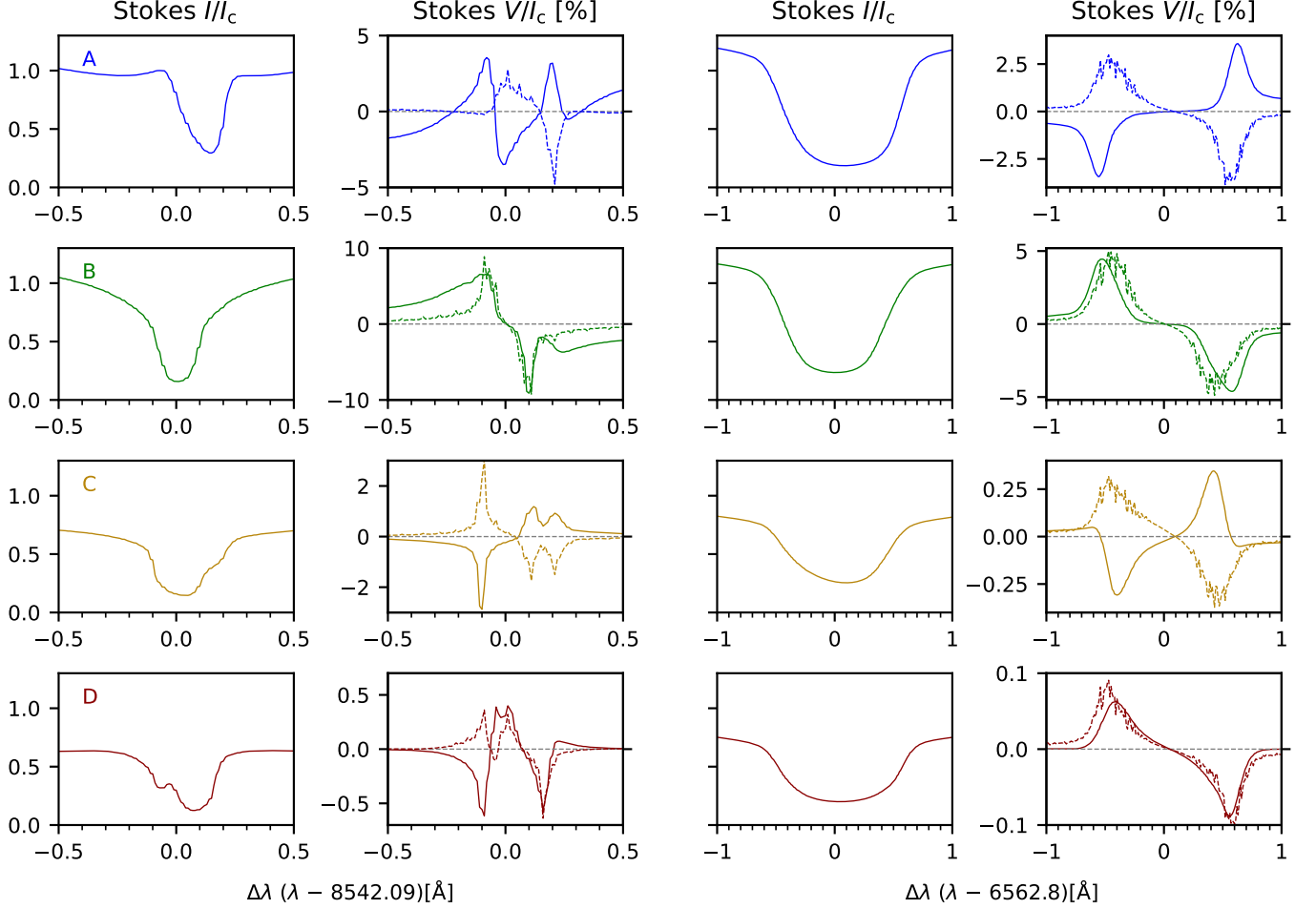


Figure 3. Stokes I/I_c and V/I_c profiles of a few selected pixels. The amplitudes of Stokes I/I_c and Stokes V/I_c are marked on ticks on the left-axis of each of the subplots. The dashed lines show the derivative of the Stokes I/I_c with the sign changed, to compare with the Stokes V/I_c . The scale of the derivatives is not shown.

the photospheric fields, while the line core samples the chromospheric fields.

The spectral profiles shown in red, pixel ‘D’, correspond to a pixel where the LOS magnetic field exhibits a negative sign in the lower chromospheric layers ($\log \tau_{500} \sim -5$) and a positive sign in the upper chromospheric layers ($\log \tau_{500} \sim -5.7$). The blue lobe of the Stokes V/I_c profile of the Ca II 8542 Å line displays a negative sign, indicating that it samples the lower chromospheric layers. Interestingly, the blue lobe of the Stokes V/I_c profile of the H α line shows a positive sign, suggesting that the H α line may probe magnetic fields at higher chromospheric heights than those sampled by the Ca II 8542 Å line.

4. METHODS OF ANALYSIS

4.1. Weak field approximation

The apparent LOS magnetic field of the Ca II 8542 Å line and H α was inferred using the weak field ap-

proximation method (WFA). We have used a spatially-coupled version of WFA developed by Morosin et al. (2020), which imposes spatial coherency in the WFA results. The magnetic field for the Ca II 8542 Å line core and the H α line core was calculated within the wavelength range of ± 0.25 Å and ± 0.15 Å, respectively. Using a narrower wavelength range (closer to line core) for the Ca II 8542 Å line does not result in sensitivity to magnetic fields higher up in the atmosphere, but it makes the measurement more noisy, so we opted to use ± 0.25 Å for this line. As discussed in section 3, the Stokes V map at the wavelength position where the amplitude of the Stokes V profile of the H α line is maximum, -0.5 Å, resembles network fields, thus shows a significant photospheric contribution. Thus, we have chosen ± 0.15 Å as the wavelength range representing the core of the H α line. Moreover, choosing a broader wavelength range for the WFA of the H α line results in photospheric contribution visible in the magnetic field

maps. Whereas, the magnetic field for the wings of the Ca II 8542 Å line and the H α line was determined over the wavelength ranges of $[-2, -1]$ Å and $[+0.35, +1.5]$ Å, respectively. More details about applying the WFA on the Ca II 8542 Å and H α lines can be found in Mathur et al. (2023, 2024).

4.2. Milne-Eddington Inversion

We performed Milne-Eddington (ME) inversions (see chapter 11 of del Toro Iniesta 2007) of the Fe I 6173 Å Stokes profiles to infer the B_{LOS} utilizing pyMilne code, a parallel C++/Python implementation¹ (de la Cruz Rodríguez 2019).

4.3. Response functions

We calculated the response functions to the B_{LOS} by perturbing the LOS magnetic field at various heights and synthesized the profiles for those perturbed atmospheres. To calculate response functions, “+” and “−” perturbations (Δx) are applied to the B_{LOS} at each height (h), resulting in the synthesized spectral line Stokes profiles, S^+ and S^- , respectively. The response of the B_{LOS} at each height is then determined by

$$RF_{B_{\text{LOS}}}(h, \lambda) = \frac{S^+ - S^-}{2 * \Delta x}. \quad (1)$$

We do not expect the magnetic field to influence the level populations; thus, for the H α line, we do not perform any iterations in the RH code, as explained in section 2. Instead, we directly apply the formal solution to compute the emergent intensity and polarization profiles for the perturbed atmospheres. For the Ca II 8542 Å and Fe I 6173 Å lines, we re-ran the RH 1.5D code for each of the perturbed atmospheres, because it was easier that way.

5. RESULTS AND DISCUSSIONS

5.1. Mapping atmospheric layers: magnetic field sensitivity of the H α line

One of the primary objectives of this study is to determine the atmospheric height at which the H α line exhibits sensitivity to the magnetic field. Additionally, we explore the H α line as a probe of the magnetic field and compare its response with the Ca II 8542 Å and Fe I 6173 Å lines to assess their diagnostic potential across different atmospheric layers. We compared the LOS magnetic field maps retrieved from all the three lines deploying various methods described in the section 4 to the actual magnetic field at different optical

depth in the simulation. Figure 4 represents the Pearson correlation coefficients between the inferred LOS magnetic fields maps and the LOS magnetic field maps at different $\log \tau_{500}$ values in the 3D MHD simulation. Additionally, the normalized mean squared difference between the inferred LOS magnetic fields and the 3D MHD model at different $\log \tau_{500}$ values is also shown. A higher Pearson correlation coefficient indicates a stronger spatial correlation between the inferred magnetic field maps and those from the 3D MHD model. Whereas, lower values of mean squared difference reflect a closer match between the inferred magnetic field amplitude and the model.

The blue-colored curve represents the LOS magnetic field derived from the Fe I 6173 Å line, showing the highest spatial correlation with the 3D MHD model at $\log \tau_{500} = -1.2$ and the lowest mean squared difference at $\log \tau_{500} = -1.3$. This aligns with the well-established understanding that Fe I lines typically sample the photospheric magnetic field (Rutten & Kostik 1982; Rutten 1988). The green-colored curve corresponds to the magnetic field map inferred using WFA from the wings of the Ca II 8542 Å line, with maximum Pearson correlation at $\log \tau_{500} = -2.6$ and the lowest mean squared difference at $\log \tau_{500} = -2.5$. In earlier studies using semi-empirical models (FALC; Avrett 1985; Fontenla et al. 1993), Centeno (2018) identified that the wings of the Ca II 8542 Å line sample photospheric layers around $\log \tau_{500} \sim -1.4$. This discrepancy may arise because Centeno (2018) employed a semi-empirical model that does not inherently include a magnetic field and applied different magnetic field stratifications in their analysis, whereas our study utilizes a realistic 3D rMHD model.

The black-colored curve reflects the maps derived from the core of the Ca II 8542 Å line, having the highest spatial correlation and minimum mean squared difference at $\log \tau_{500} = -5.1$. According to Centeno (2018), the core of the Ca II 8542 Å line is sensitive around $\log \tau_{500} = -5.3$.

In contrast to the Fe I 6173 Å and Ca II 8542 Å lines, the magnetic field map retrieved from the wings of the H α line (brown curve) shows spatial correlation and the lowest mean squared difference at notably different $\log \tau_{500}$ values, specifically -3 and -4.2 , respectively. The higher spatial correlation at $\log \tau_{500} = -3$ suggests influence from upper photospheric or lower chromospheric layers, while the minimum mean squared difference at $\log \tau_{500} = -4.2$ indicates some contribution from even higher layers. Therefore it suggests that magnetic field inferred from the H α wings might sample a range of the atmosphere making its interpretation more complex. The core of the H α line shows the highest spa-

¹ <https://github.com/jaimedelacruz/pyMilne>

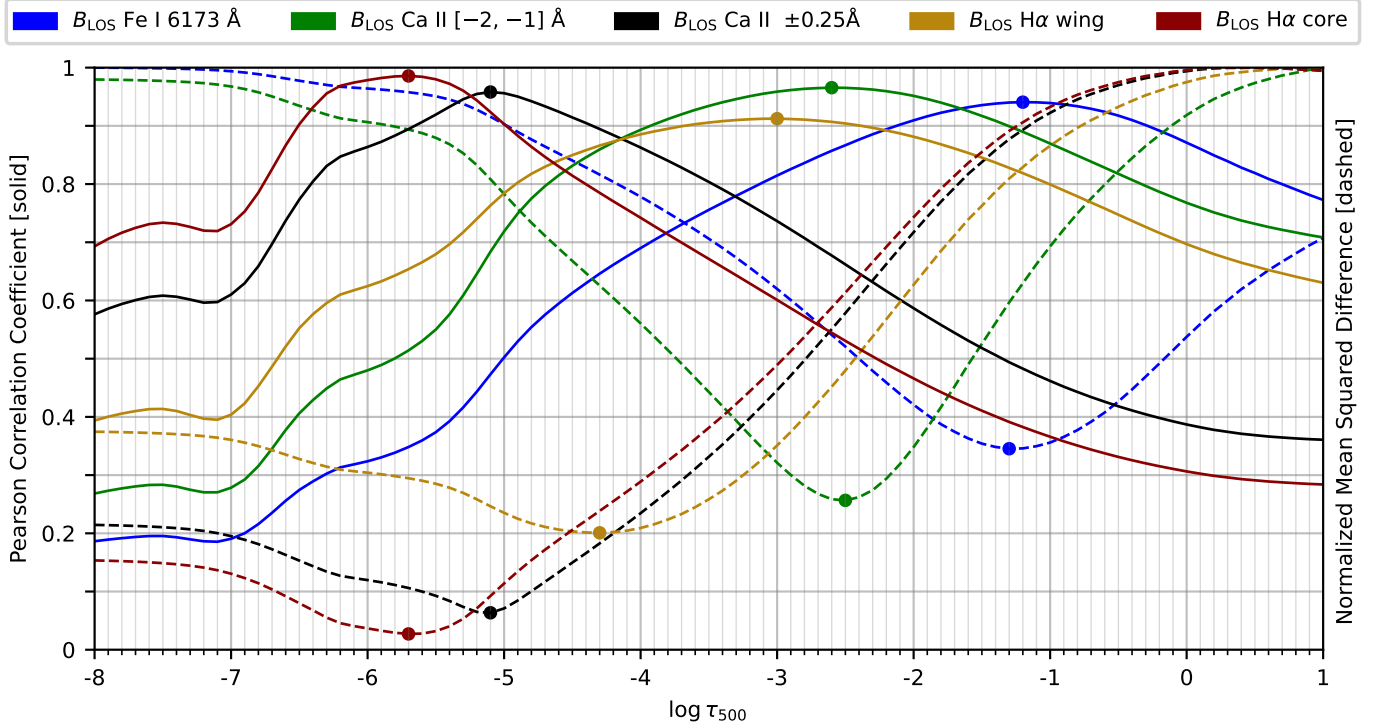


Figure 4. Pearson correlation (solids) and normalized mean squared difference (dashed) of the inferred magnetic fields with the 3D MHD model at different $\log \tau_{500}$ values.

tial correlation and lowest mean squared difference both at $\log \tau_{500} = -5.7$, suggesting that the LOS magnetic field maps inferred from the $H\alpha$ line core consistently probe chromospheric magnetic fields at greater heights than those probed by the Ca II 8542 Å line core ($\log \tau_{500} = -5.1$).

With the above analysis, we conclude that $H\alpha$ line core and wings sample the LOS magnetic field around $\log \tau_{500} = -5.7$ and $\log \tau_{500} = -3.0$, respectively. In comparison, the Ca II 8542 Å line core and wings are more sensitive to the LOS magnetic field around $\log \tau_{500} = -5.1$ and $\log \tau_{500} = -2.6$, respectively. The LOS magnetic field inferred using the Milne-Eddington inversion of the Fe I 6173 Å line represents the magnetic field at $\log \tau_{500} = -1.2$. In Fig. 5 and 6, we compare the LOS magnetic field maps inferred from the synthetic observables with that of the ground truth, the 3D MHD model. The morphology of the LOS magnetic field derived from Fe I 6173 Å, as well as from the wings and core of the Ca II 8542 Å line, aligns closely with the LOS magnetic field maps at layers where the Pearson correlation is highest. The scatter plots in the third column indicate that the inferred amplitudes correspond well with the model, with slopes close to unity. The rms differences between the inferred maps and the 3D MHD model are 40 G for Fe I 6173 Å, 20 G for the wings of Ca II 8542 Å, and 10 G for the core of Ca II 8542 Å.

The LOS magnetic field inferred from the wings of the $H\alpha$ line shows a weak correlation with the layer at which the Pearson correlation is highest, especially when compared to the maps derived from the Fe I 6173 Å and Ca II 8542 Å lines, and exhibits lower amplitudes than the 3D MHD model. This finding is also reflected in the scatter plot in the third column, which displays a significant scatter and a slope of around 0.5. However, the rms differences, approximately 40 G, are comparable to those in the maps inferred from the Fe I 6173 Å and Ca II 8542 Å lines. The correlation with the lower chromospheric / upper photospheric layers, $\log \tau_{500} = -3$, though with lower field amplitudes, suggests the contribution of photospheric fields in addition to chromospheric fields within the Stokes V profiles of the wings of the $H\alpha$ line.

The LOS magnetic field maps inferred from the core of the $H\alpha$ line, unlike those from the wings, exhibit a strong spatial correlation and similar amplitudes to the $\log \tau_{500} = -5.7$ layer of the 3D MHD model. This is also evident in the scatter plot in the third column, which shows a unity slope and rms differences of just 3 G. This result strongly supports the hypothesis that the core of the $H\alpha$ line consistently probes the chromospheric magnetic field at higher layers than the Ca II 8542 Å line, which probes $\log \tau_{500} \sim -5$.

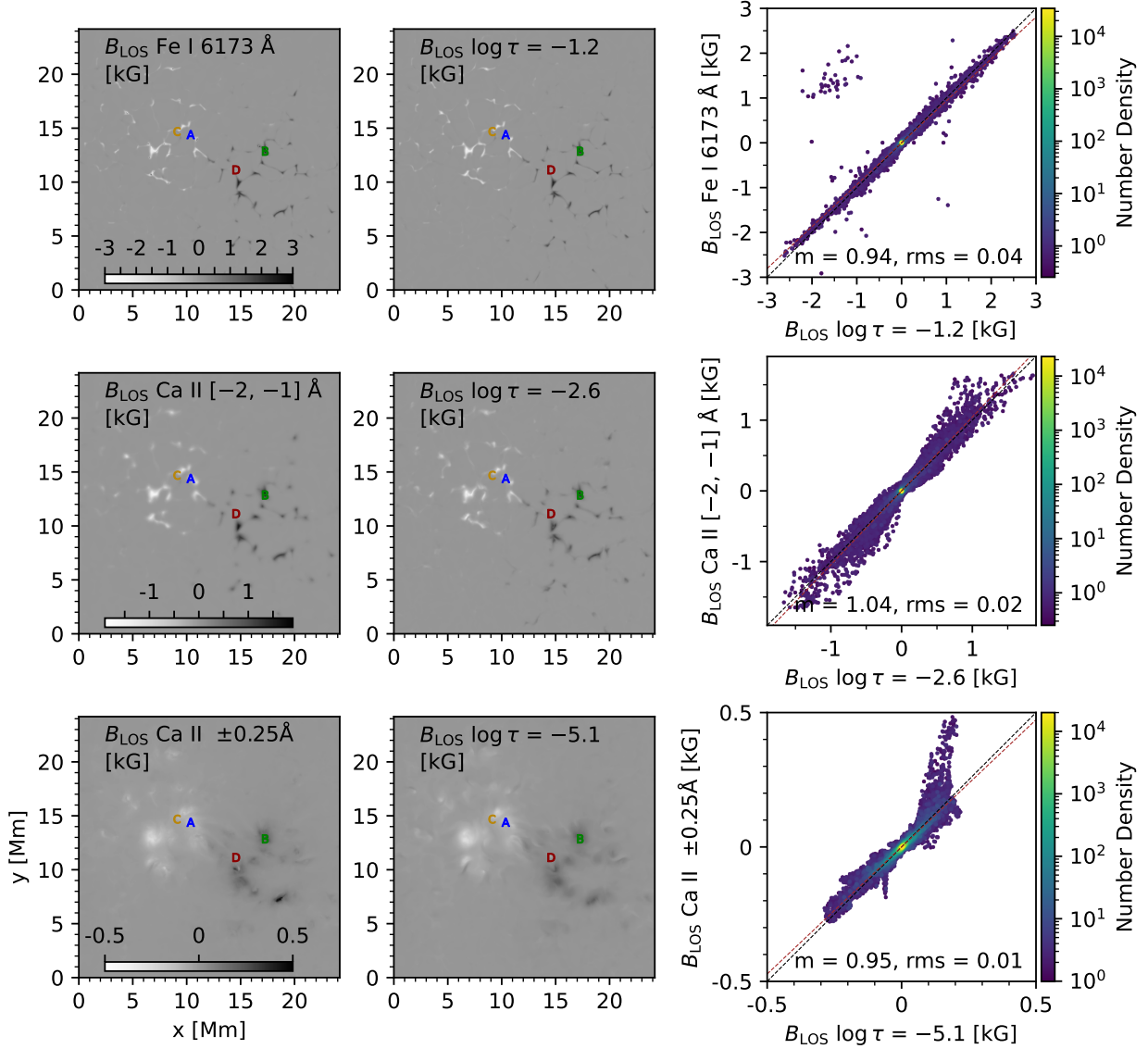


Figure 5. Comparison of magnetic fields inferred from Fe I 6173 Å and Ca II 8542 Å lines with those of the 3D MHD model. The first column shows magnetic field maps derived from synthetic observables. The second column displays LOS magnetic field maps from the 3D MHD model at the atmospheric layer at which the corresponding maps in the first column show the best correlation (see Fig. 4). The final column presents a 2D histogram between the maps in the first and second columns. The slope of the linear regression of the scatter plot in the third column is indicated by m and rms indicates the root mean square of the difference between the two values.

To assess the effect of noise in high-resolution ground-based solar observations, we simulate realistic noise conditions and re-infer magnetic fields using the weak-field approximation. While the $H\alpha$ maps appear noisier due to weaker polarization signals, the magnetic structures remain discernible, with an rms error of 18 G, and the scatter decreases with increasing field strength—indicating strong potential for application in active regions. More details are provided in appendix B.

5.2. Analysis of response functions and formation height of polarization profiles of the $H\alpha$ line

To determine the optical depths (heights) where the Stokes V profile of the $H\alpha$ line is most sensitive to the LOS magnetic field, we analyzed the response functions of the $H\alpha$, Ca II 8542 Å, and Fe I 6173 Å lines for a few representative pixels marked in Fig. 2. The maximum response of these lines occurs at different $\log \tau_{500}$ values: $H\alpha$ line core at -5.9 to -5.6 , Ca II 8542 Å line at -5.7 to -5.1 , and Fe I 6173 Å line at -1.2 . For pixels with simple magnetic field stratification (same polarity across heights), the inferred LOS magnetic field closely matches the rMHD model at the $\log \tau_{500}$ with maximum response. However, for pixels with complex stratifica-

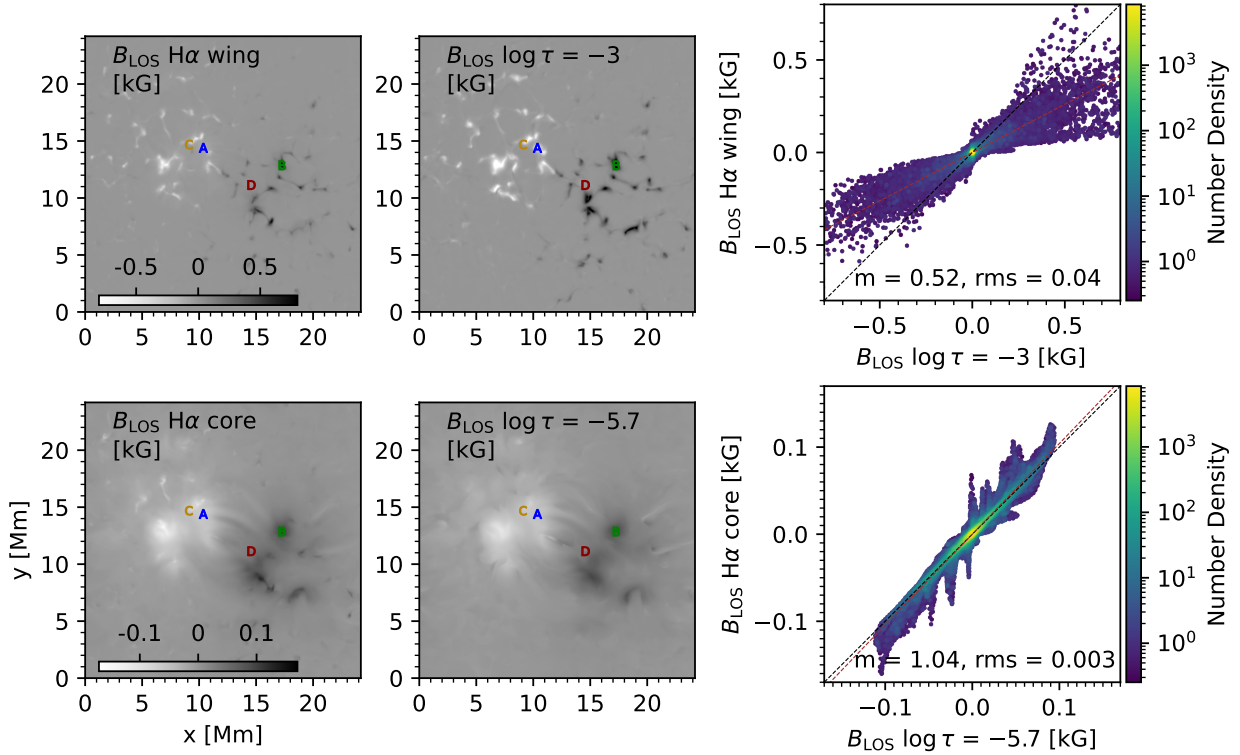


Figure 6. Comparison of magnetic fields inferred from H α line with that of the 3D MHD model in the same format as in Fig. 5.

tion (steep gradients and polarity reversals), the inferred field remains close to the rMHD model but may differ from the value of rMHD model at the $\log \tau_{500}$ with maximum response. This shift is attributed to the complex Stokes I and V profiles observed in these regions. The temperature structure and the velocity fields may have contributed to the formation of such profiles in addition to the stratification of the LOS magnetic fields. Overall, the analysis shows that the Stokes V profiles of the H α line core are sensitive to magnetic field perturbations at higher atmospheric layers than those of the Ca II 8542 Å line. Consequently, the H α line core probes the LOS magnetic field at higher layers than that inferred from the Ca II 8542 Å line. A detailed analysis, including the response functions and magnetic field stratifications for individual pixels, is provided in Appendix A.

In Fig. 7, we show an histogram of difference between the height at $\log \tau_{500} = -5.7$ with the height at $\log \tau_{500} = -5.1$. This difference can be as minimal as 100 km and can be as high as 1800 km. On average, this difference is about 500 km. Thus, it clearly shows that the Stokes V profiles of the H α line core form on average 500 km above that of the Ca II 8542 Å line.

6. SUMMARY AND CONCLUSIONS

We have investigated whether the Stokes I and V profiles of the H α line probe the chromospheric magnetic

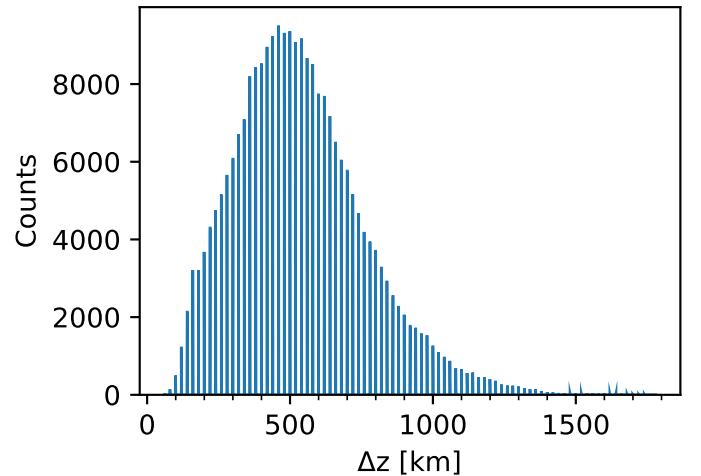


Figure 7. Histogram showing the difference of height of formation between the H α and Ca II line.

field. We modeled the Stokes I and V profiles of the H α line using 3D radiative transfer using the field-free approximation and compared the LOS magnetic field inferred with the 3D rMHD model used. In addition to the H α line, we have also synthesized the Stokes I and V profiles of the Ca II 8542 Å and Fe I 6173 Å lines, for comparison.

The Pearson correlation coefficient between the LOS magnetic field map inferred from the H α line core and

the rMHD model is highest at $\log \tau_{500} = -5.7$, whereas for the Ca II 8542 Å line core, the highest correlation occurs at $\log \tau_{500} = -5.1$. This is clear evidence in support of conclusions from earlier observational studies, Mathur et al. (2023) and Mathur et al. (2024), that the H α line core consistently probes chromospheric magnetic field at higher layers than the Ca II 8542 Å line.

The changes in the polarity of the LOS magnetic field across different layers of the solar atmosphere are reflected on the Stokes V profiles of the H α and Ca II 8542 Å lines. When the magnetic field changes sign from the photosphere to the chromosphere, we observe that the sign of the Stokes V also changes from the line wings to the line core. Similarly and interestingly, when there was a change in polarity at different heights of the solar chromosphere, the blue lobe of the Stokes V profiles of the H α and Ca II 8542 Å line core had different signs.

In contrast to the H α line core, the map of the LOS magnetic field inferred from the wings of the H α line had higher spatial correlation at $\log \tau_{500} = -3$, whereas the minimum mean squared difference was at $\log \tau_{500} = -4.2$. This suggests that the H α line wings have significant contributions from both photosphere and chromospheric heights, making it challenging to interpret.

The study of the response functions also confirms that the maximum sensitivity of the Stokes V profiles of the H α line core to the perturbations of the LOS magnetic field is at higher atmospheric layers ($\log \tau_{500} \in [-5.9, -5.6]$) than the Ca II 8542 Å line ($\log \tau_{500} \in [-5.7, -5.1]$). On average, the Stokes V profiles of the H α line core forms about +500 km above the Stokes V profiles of the Ca II 8542 Å line, ranging from +100 to +1800 km. Adding noise at the level of $10^{-3}I_c$ produces noisier H α polarization maps, but we find that

most simulated magnetic structures remain visible. The method is robust even for weaker fields.

In summary, the Stokes V profiles of the H α line core always probe the chromospheric magnetic field at higher layers than the Ca II 8542 Å line. Spectropolarimetric observations of the H α line when recorded simultaneously with widely used chromospheric diagnostics such as the Ca II 8542 Å line can provide complementary insights into the stratification of the magnetic field by probing LOS magnetic field at higher layers than the Ca II 8542 Å line. Instruments like the Visible Spectropolarimeter (de Wijn et al. 2022) on the Daniel K. Inouye Solar Telescope (Rimmele et al. 2020) offer the capability to conduct such simultaneous observations.

This research has made use of the High-Performance Computing (HPC) resources (NOVA cluster) made available by the Computer Center of the Indian Institute of Astrophysics, Bangalore. J.J. acknowledges financial support from the Science and Engineering Research Board (SERB)/Anusandhan National Research Foundation (ANRF), India, under the Core Research Grant (CRG), Grant No. CRG/2023/007464. This work has been supported by the Research Council of Norway through its Centers of Excellence scheme, project number 262622. Computational resources have been provided by UNINETT Sigma2 - the National Infrastructure for High Performance Computing and Data Storage in Norway. This research has made use of NASA's Astrophysics Data System Bibliographic Services. We have also used the packages h5py (Collette 2013), matplotlib (Hunter 2007), and NumPy (Harris et al. 2020) to carry out our data analysis.

Software: NumPy(Harris et al. 2020), matplotlib(Hunter 2007), RH(Uitenbroek 2001), Multi3d(Leenaarts & Carlsson 2009), h5py (Collette 2013), pyMilne(de la Cruz Rodríguez 2019), Spatial-WFA(Morosin et al. 2020)

REFERENCES

- Abdussamatov, H. I. 1971, SoPh, 16, 384, doi: [10.1007/BF00162480](https://doi.org/10.1007/BF00162480)
- Avrett, E. H. 1985, in Chromospheric Diagnostics and Modelling, ed. B. W. Lites, 67–127
- Balasubramaniam, K. S., Christopoulou, E. B., & Uitenbroek, H. 2004, ApJ, 606, 1233, doi: [10.1086/383118](https://doi.org/10.1086/383118)
- Bjørgen, J. P., Leenaarts, J., Rempel, M., et al. 2019, A&A, 631, A33, doi: [10.1051/0004-6361/201834919](https://doi.org/10.1051/0004-6361/201834919)
- Carlsson, M., Hansteen, V. H., Gudiksen, B. V., Leenaarts, J., & De Pontieu, B. 2016, A&A, 585, A4, doi: [10.1051/0004-6361/201527226](https://doi.org/10.1051/0004-6361/201527226)
- Carlsson, M., & Stein, R. F. 2002, ApJ, 572, 626, doi: [10.1086/340293](https://doi.org/10.1086/340293)
- Centeno, R. 2018, ApJ, 866, 89, doi: [10.3847/1538-4357/aae087](https://doi.org/10.3847/1538-4357/aae087)
- Collette, A. 2013, Python and HDF5 (O'Reilly)
- de la Cruz Rodríguez, J. 2019, A&A, 631, A153, doi: [10.1051/0004-6361/201936635](https://doi.org/10.1051/0004-6361/201936635)

- de Wijn, A. G., Casini, R., Carlile, A., et al. 2022, *SoPh*, 297, 22, doi: [10.1007/s11207-022-01954-1](https://doi.org/10.1007/s11207-022-01954-1)
- del Toro Iniesta, J. C. 2007, *Introduction to Spectropolarimetry*
- Fontenla, J. M., Avrett, E. H., & Loeser, R. 1993, *ApJ*, 406, 319, doi: [10.1086/172443](https://doi.org/10.1086/172443)
- Gudiksen, B. V., Carlsson, M., Hansteen, V. H., et al. 2011, *A&A*, 531, A154, doi: [10.1051/0004-6361/201116520](https://doi.org/10.1051/0004-6361/201116520)
- Hanaoka, Y. 2005, *PASJ*, 57, 235, doi: [10.1093/pasj/57.1.235](https://doi.org/10.1093/pasj/57.1.235)
- Harris, C. R., Millman, K. J., van der Walt, S. J., et al. 2020, *Nature*, 585, 357, doi: [10.1038/s41586-020-2649-2](https://doi.org/10.1038/s41586-020-2649-2)
- Hunter, J. D. 2007, *Computing in Science & Engineering*, 9, 90, doi: [10.1109/MCSE.2007.55](https://doi.org/10.1109/MCSE.2007.55)
- Jaume Bestard, J., Trujillo Bueno, J., Bianda, M., Štěpán, J., & Ramelli, R. 2022, *A&A*, 659, A179, doi: [10.1051/0004-6361/202141834](https://doi.org/10.1051/0004-6361/202141834)
- Joshi, J., & Rouppe van der Voort, L. H. M. 2022, *A&A*, 664, A72, doi: [10.1051/0004-6361/202243051](https://doi.org/10.1051/0004-6361/202243051)
- Kurucz, R. L. 2011, *Canadian Journal of Physics*, 89, 417, doi: [10.1139/p10-104](https://doi.org/10.1139/p10-104)
- Lagg, A., Lites, B., Harvey, J., Gosain, S., & Centeno, R. 2017, *SSRv*, 210, 37, doi: [10.1007/s11214-015-0219-y](https://doi.org/10.1007/s11214-015-0219-y)
- Landi Degl’Innocenti, E., & Landolfi, M. 2004, *Polarization in Spectral Lines*, Vol. 307, doi: [10.1007/978-1-4020-2415-3](https://doi.org/10.1007/978-1-4020-2415-3)
- Leenaarts, J., & Carlsson, M. 2009, in *Astronomical Society of the Pacific Conference Series*, Vol. 415, *The Second Hinode Science Meeting: Beyond Discovery-Toward Understanding*, ed. B. Lites, M. Cheung, T. Magara, J. Mariska, & K. Reeves, 87
- Leenaarts, J., Carlsson, M., & Rouppe van der Voort, L. 2012, *ApJ*, 749, 136, doi: [10.1088/0004-637X/749/2/136](https://doi.org/10.1088/0004-637X/749/2/136)
- López Ariste, A., Casini, R., Paletou, F., et al. 2005, *ApJL*, 621, L145, doi: [10.1086/429158](https://doi.org/10.1086/429158)
- Mathur, H., Joshi, J., Nagaraju, K., Rouppe van der Voort, L., & Bose, S. 2022, *A&A*, 668, A153, doi: [10.1051/0004-6361/202244332](https://doi.org/10.1051/0004-6361/202244332)
- Mathur, H., Nagaraju, K., Joshi, J., & de la Cruz Rodríguez, J. 2023, *ApJ*, 946, 38, doi: [10.3847/1538-4357/acbf49](https://doi.org/10.3847/1538-4357/acbf49)
- Mathur, H., Nagaraju, K., Yadav, R., & Joshi, J. 2024, *ApJ*, 971, 30, doi: [10.3847/1538-4357/ad54ba](https://doi.org/10.3847/1538-4357/ad54ba)
- Morosin, R., de la Cruz Rodríguez, J., Vissers, G. J. M., & Yadav, R. 2020, *A&A*, 642, A210, doi: [10.1051/0004-6361/202038754](https://doi.org/10.1051/0004-6361/202038754)
- Nagaraju, K., Sankarasubramanian, K., & Rangarajan, K. E. 2008, *ApJ*, 678, 531, doi: [10.1086/533433](https://doi.org/10.1086/533433)
- . 2020, *Journal of Astrophysics and Astronomy*, 41, 10, doi: [10.1007/s12036-020-9627-9](https://doi.org/10.1007/s12036-020-9627-9)
- Pastor Yabar, A., Martínez González, M. J., & Collados, M. 2020, *A&A*, 635, A210, doi: [10.1051/0004-6361/202037480](https://doi.org/10.1051/0004-6361/202037480)
- Przybilla, N., & Butler, K. 2004, *ApJ*, 609, 1181, doi: [10.1086/421316](https://doi.org/10.1086/421316)
- Rempel, M. 2012, *ApJ*, 750, 62, doi: [10.1088/0004-637X/750/1/62](https://doi.org/10.1088/0004-637X/750/1/62)
- Rimmele, T. R., Warner, M., Keil, S. L., et al. 2020, *SoPh*, 295, 172, doi: [10.1007/s11207-020-01736-7](https://doi.org/10.1007/s11207-020-01736-7)
- Rutten, R. J. 1988, in *Astrophysics and Space Science Library*, Vol. 138, *IAU Colloq. 94: Physics of Formation of Fe II Lines Outside LTE*, ed. R. Viotti, A. Vittone, & M. Friedjung, 185–210, doi: [10.1007/978-94-009-4023-9_23](https://doi.org/10.1007/978-94-009-4023-9_23)
- Rutten, R. J., & Kostik, R. I. 1982, *A&A*, 115, 104
- Smitha, H. N., van Noort, M., Solanki, S. K., & Castellanos Durán, J. S. 2023, *A&A*, 669, A144, doi: [10.1051/0004-6361/202245130](https://doi.org/10.1051/0004-6361/202245130)
- Socas-Navarro, H., & Uitenbroek, H. 2004, *ApJL*, 603, L129, doi: [10.1086/383147](https://doi.org/10.1086/383147)
- Uitenbroek, H. 2001, *ApJ*, 557, 389, doi: [10.1086/321659](https://doi.org/10.1086/321659)
- Vögler, A., Shelyag, S., Schüssler, M., et al. 2005, *A&A*, 429, 335, doi: [10.1051/0004-6361:20041507](https://doi.org/10.1051/0004-6361:20041507)
- Štěpán, J., & Trujillo Bueno, J. 2010, *Mem. Soc. Astron. Italiana*, 81, 810, <https://arxiv.org/abs/1001.2720>
- . 2011, *ApJ*, 732, 80, doi: [10.1088/0004-637X/732/2/80](https://doi.org/10.1088/0004-637X/732/2/80)
- Yadav, R., Díaz Baso, C. J., de la Cruz Rodríguez, J., Calvo, F., & Morosin, R. 2021, *A&A*, 649, A106, doi: [10.1051/0004-6361/202039857](https://doi.org/10.1051/0004-6361/202039857)

APPENDIX

A. DETAILED ANALYSIS OF RESPONSE FUNCTIONS

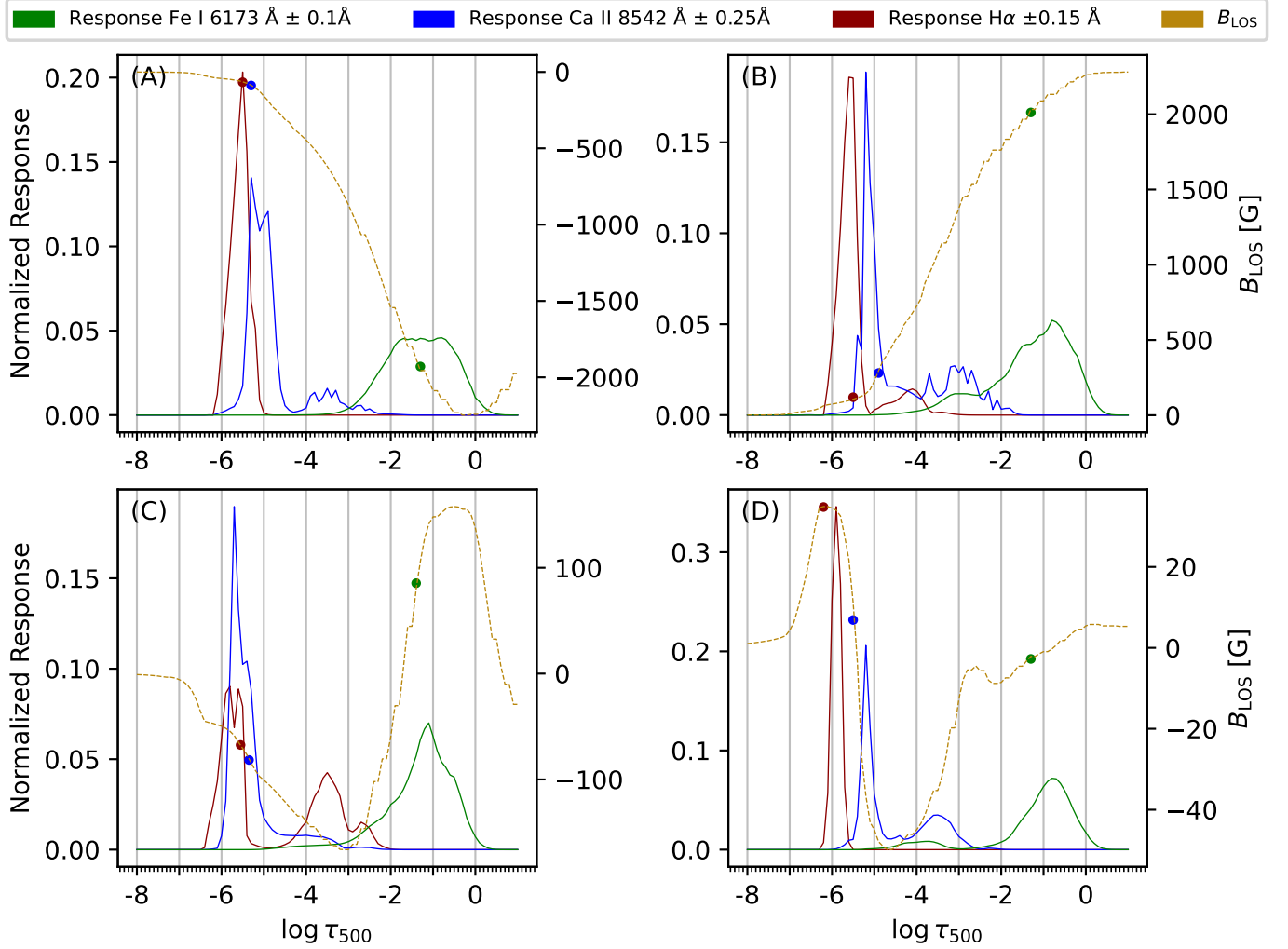


Figure 8. Wavelength integrated normalized response functions of the Stokes V profiles to the perturbations of the LOS magnetic field for the Fe I 6173 Å, Ca II 8542 Å and H α lines. The response functions for the profiles for the 4-selected pixels shown in Fig. 3 are shown in panels (A), (B), (C) and (D), respectively. The stratification of the B_{LOS} is also shown for completeness. The value of the LOS magnetic field inferred from the H α , Ca II 8542 Å and Fe I 6173 Å spectral lines is overplotted with \bullet at $\log \tau_{500}$ values with closest match with the rMHD model, in the same color scheme as the spectral lines.

To determine the optical depths (heights) at which the Stokes V profile of the H α line is most sensitive to the magnetic field, we have analyzed the response of the Stokes V profiles to the perturbations of the LOS magnetic field. The details about the calculation of the response functions are mentioned in section 4.3. In Fig. 8, we show wavelength-integrated response functions of the Stokes V profiles to the perturbations of the LOS magnetic field for the Fe I 6173 Å (green-colored curve) line, Ca II 8542 Å (blue-colored curve) line, and the H α (red-colored curve) line, for the 4-selected pixels marked in Fig. 2. The integration wavelength range is set to ± 0.1 Å for the Fe I 6173 Å line, ± 0.25 Å for the Ca II 8542 Å line, and ± 0.15 Å for the H α line. For comparison, the stratification of the LOS magnetic field from the 3D MHD model is overplotted (brown-colored curve) and the scale is marked on the right-axis.

The magnetic field values inferred from the synthetic spectral profiles of the $H\alpha$, Ca II 8542 Å and Fe I 6173 Å lines with • at $\log \tau_{500}$ values with the closest match with the rMHD model are also indicated.

In panels (A) and (B), we show the response functions of the Stokes V profiles to the perturbations of the LOS magnetic field for pixels where the magnetic field is consistently positive (or negative) polarity across all atmospheric heights. The $H\alpha$ line exhibits its peak sensitivity to LOS magnetic field perturbations at $\log \tau_{500} = -5.6$, while the Ca II 8542 Å line reaches its maximum response at $\log \tau_{500} = -5.1$. For the Fe I 6173 Å line, the peak response occurs at $\log \tau_{500} = -1.2$. The LOS magnetic field inferred from the $H\alpha$, Ca II 8542 Å, and Fe I 6173 Å lines closely match with the value of the rMHD model at the $\log \tau_{500}$ values at which their respective response functions are maximum.

The atmospheres of the remaining two selected pixels exhibit complex LOS magnetic field stratification, characterized by steep gradients and polarity changes with height, as shown in panels (C) and (D). In the atmosphere of the pixel shown in panel (C), the LOS magnetic field is positive in the lower photospheric layers ($\log \tau_{500} > -1.8$) and negative in the upper photospheric and chromospheric layers ($\log \tau_{500} < -1.8$). Whereas, in the atmosphere of the pixel shown in panel (D), the LOS magnetic field is negative in the photosphere and lower chromosphere ($\log \tau_{500} > -5.4$) and positive in the upper chromosphere ($\log \tau_{500} < -5.4$).

In the case shown in panel (C), where the LOS magnetic field exhibits opposite polarities in the lower photosphere and chromosphere, the $H\alpha$ and Ca II 8542 Å lines exhibit peak responses to LOS magnetic field perturbations around $\log \tau_{500} = -5.8$ and -5.7 , respectively. Additionally, the $H\alpha$ line displays a notable response around $\log \tau_{500} = -3.5$. The Fe I 6173 Å line peaks around $\log \tau_{500} = -1.2$. The inferred LOS magnetic fields from the $H\alpha$, Ca II 8542 Å and Fe I 6173 Å lines closely match with the rMHD model, however, they differ from the values of the rMHD model at the $\log \tau_{500}$ where the corresponding response is maximum.

For the case shown in panel (D), where the LOS magnetic field has opposite polarities in the lower and upper chromosphere, the $H\alpha$ line exhibits peak response to LOS magnetic field perturbations at $\log \tau_{500} = -5.9$. While the Ca II 8542 Å and the Fe I 6173 Å lines peak at $\log \tau_{500} = -5.1$ and -0.8 , respectively. Similar to the scenario depicted in panel (C), the LOS magnetic field values inferred from the $H\alpha$, Ca II 8542 Å, and Fe I 6173 Å lines are different compared to the value of the rMHD model at the $\log \tau_{500}$ where their respective response functions are maximum.

As discussed in section 5.1 and shown in Fig. 4, the LOS magnetic field map inferred from the $H\alpha$ line core closely corresponds to the rMHD model at $\log \tau_{500} = -5.7$. However, the analysis of the response functions suggests that, for individual pixels, the maximum response of the Stokes V profile to LOS magnetic field perturbations can occur at different $\log \tau_{500}$ values, depending on the magnetic field stratification.

For relatively simple stratifications, where the LOS magnetic field maintains the same polarity with height, the inferred magnetic field closely matches the value of the rMHD model at the $\log \tau_{500}$ where the response is maximum. In contrast, for pixels with complex stratification—characterized by steep gradients and polarity reversals—the inferred LOS magnetic field remains close to the rMHD model but may be different than the value of the rMHD model at the $\log \tau_{500}$ with the maximum response. This discrepancy may result from the complex Stokes I and V profiles observed for these pixels, see brown and red-colored Stokes I/I_c and Stokes V/I_c profiles of the Ca II 8542 Å line of Fig. 3. In addition to the complex LOS magnetic field stratification, the temperature structure and the velocity fields may have contributed to the formation of such profiles. Interestingly, for the pixel in panel (D), restricting the WFA analysis of the Ca II 8542 Å line to only the blue wing range ($[-0.25, 0]$ Å) yields a LOS magnetic field of approximately -20 G, which corresponds to the value of the rMHD model at the $\log \tau_{500}$ of maximum response (-5.1).

Overall, the response function analysis clearly demonstrates that the maximum response of the Stokes V profiles of the $H\alpha$ line to the perturbations of the LOS magnetic field occurs at higher atmospheric layers than that of the Ca II 8542 Å line. Consequently, the LOS magnetic fields inferred from the Stokes V profiles of the $H\alpha$ line core are from higher atmospheric layers compared to those inferred from Ca II 8542 Å line.

B. VALIDATION OF WFA UNDER SIMULATED NOISE CONDITIONS

To estimate the effect of noise in high-resolution ground-based observations, we introduce Gaussian noise with a standard deviation of $\sigma = 10^{-3}I_c$ into the synthetic Stokes profiles and re-infer the LOS magnetic field maps using the WFA, following the same procedure as in Fig. 5 and 6. Figure 9 displays the resulting inferred maps, accompanied by scatter plots comparing the fields retrieved from the noise-free and noise-degraded profiles. For the Ca II 8542 Å line, the magnetic field maps derived from the noise-degraded profiles show minimal deviation from those obtained in the noise-free case. This robustness is likely due to the relatively stronger Stokes V/I_c signals in the Ca II 8542 Å line, which reach amplitudes of approximately 10%. In contrast, the $H\alpha$ maps exhibit significantly more noise when

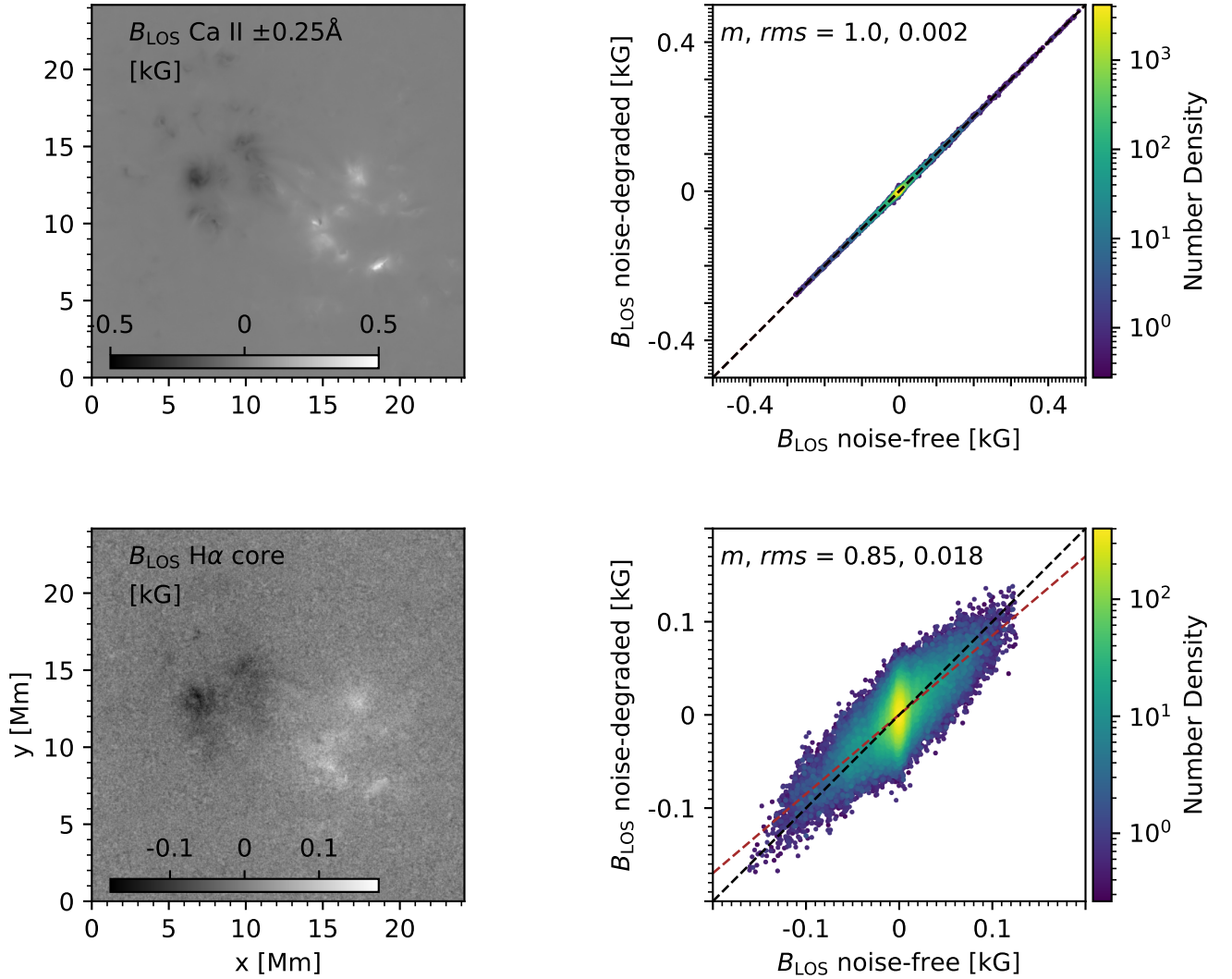


Figure 9. Top-left: Map of the line-of-sight magnetic field inferred from the Ca II 8542 Å line using the WFA applied to synthetic Stokes profiles degraded with Gaussian noise ($\sigma = 10^{-3}I_c$). Top-right: Scatter plot comparing WFA-inferred B_{LOS} from noise-free versus noise-degraded Ca II 8542 Å profiles. Bottom panels: Same as top, but for the Hα line. The slope of the linear regression of the scatter plot in the third column is indicated by m and rms indicates the root mean square of the difference between the two values.

inferred from noise-degraded profiles. We attribute this to the inherently weaker Stokes V/I_c amplitudes in Hα line, which are on the order of $\sim 0.2\%$. Despite the increased noise, the underlying magnetic structures remain discernible and coherent. The rms error between the noise-degraded and noise-free maps in the Hα case is found to be 18 G. Notably, the scatter decreases with increasing field strength. It is important to highlight that the noisiness of the Hα magnetic field map primarily arises from the properties of the underlying simulation, which models an enhanced network quiet-Sun atmosphere with maximum field strengths of only ~ 110 G at $\log \tau_{500} = -5.7$. In observational scenarios involving stronger magnetic fields, such as active regions studied by Mathur et al. (2023, 2024), where chromospheric field strengths can reach 500–1000 G, the polarization signals would be substantially stronger and more reliably detected.